Nanoscale

PAPER

View Article Online
View Journal

Cite this: DOI: 10.1039/c8nr01573b

Ultrafast saturable absorption in TiS_2 induced by non-equilibrium electrons and the generation of a femtosecond mode-locked laser†

Xiangling Tian,[a] Rongfei Wei,[b] Meng Liu,[c] Chunhui Zhu,[d] Zhichao Luo,[c] Fengqiu Wang[d] and Jianrong Qiu*[a,e]

Received 24th February 2018,
Accepted 30th April 2018

DOI: 10.1039/c8nr01573b

rsc.li/nanoscale

Non-equilibrium electrons induced by ultrafast laser excitation in a correlated electron material can disturb the Fermi energy as well as optical nonlinearity. Here, non-equilibrium electrons translate a semiconductor TiS_2 material into a plasma to generate broad band nonlinear optical saturable absorption with a sub-picosecond recovery time of ~768 fs (corresponding to modulation frequencies over 1.3 THz) and a modulation response up to ~145%. Based on this optical nonlinear modulator, a stable femtosecond mode-locked pulse with a pulse duration of ~402 fs and a pulse train with a period of ~175.5 ns is observed in the all-optical system. The findings indicate that non-equilibrium electrons can promote a TiS_2-based saturable absorber to be an ultrafast switch for a femtosecond pulse output.

Introduction

Nonlinear optical (NLO) effects give rise to lots of modern photonic functionalities, including frequency mixing processes, Kerr effects, the generation of ultrashort pulses, all-optical signal processing and saturable absorption (SA).[1–5] Optical nonlinearities are inherently weak because they describe the interaction of light with matter that accompanies the nonlinear response of materials to an applied electromagnetic field with respect to the amplitude regime.[3] There is an increased consensus that the discovery of nonlinear optical materials which show a strong interaction between light and matter can be very significant in both fundamental science and for industrial applications.

In materials showing saturable absorption, optical transmittance increases after intense laser irradiation. One approach for the application of these materials is to serve as a saturable absorber to generate high-peak-power and/or ultrashort fiber laser pulses *via* passive Q-switching and/or mode-locking, particularly in the infrared (NIR) and mid-infrared region.[6,7] At present, because of the outstanding performance and ultrafast carrier dynamics, graphene[8,9] and its analogues, for example transition metal dichalcogenides (TMDCs),[10,11] topological insulators (TI),[12] and black phosphorous (BP)[13] provide new interest for mode-locked lasers in fiber-based systems. However, they have the drawbacks of a low absorption coefficient (for graphene),[8] a response region near 1.5–2.0 eV (for TMDCs including MoS_2, WS_2, $MoSe_2$, and WSe_2),[10,11] insulated bulk states (for TI), as well as being easily oxidized under ambient conditions (for BP).[13] In order to obtain a high on/off ratio and the mobility for optoelectronic application, these materials are usually limited to few-layer regimes (<10 layers),[8–11,14–20] which misleads the focus of NLO studies to monolayer or few-layer materials, ignoring the inherent weakness in optical nonlinearities. According to the report by Xiong *et al.*, the interaction between light and matter is the strongest under a thickness of ~70 nm.[21,22] Recently, Yu *et al.* reported a modulation depth of 27% and passively Q-switched laser generation using a broadband 30 MoS_2 layer saturable absorber.[23] More importantly, Yong Min Jhon *et al.* reported femtosecond laser mode-locking using 'bulk-structured' WTe_2 with 100–200 layers (corresponding to 80–150 nm) to increase the coupling of light and WTe_2.[14] The introduction of these 'bulk' materials may be used as an approach to increase the coupling between light and matter. Up to now, the interaction between non-equilibrium electrons and an electromagnetic field of light to

[a]State Key Laboratory of Luminescent Materials and Devices and School of Materials Science and Engineering, South China University of Technology, Wushan Road 381, Guangzhou 510641, PR China
[b]Department of Physics, Zhejiang Normal University, Jinhua, Zhejiang, 321004, PR China
[c]School of Information and Optoelectronic Science and Engineering, South China Normal University, Guangzhou, Guangdong 510006, China
[d]School of Electronic Science and Engineering, Nanjing University, Nanjing 210093, China
[e]State Key Laboratory of Modern Optical Instrumentation, College of Materials Science and Engineering, Zhejiang University, Hangzhou, Zhejiang 310027, PR China. E-mail: qjr@zju.edu.cn

†Electronic supplementary information (ESI) available. See DOI: 10.1039/c8nr01573b

enhance the NLO response has only been investigated in plasmonic nanocrystals (noble metals such as gold, silver, and copper; heavily doped colloidal plasmonic nanocrystals such as $Cu_{2-x}S$, $Cu_{2-x}Se$, and $Cu_{2-x}Te$)[24–26] and transparent conducting oxides (ITO films/nanorod arrays and Al-doped ZnO).[27,28] However, despite similar investigations (absorption response near the band edge) in monolayer semiconductors,[29] the NLO response induced by non-equilibrium electrons is still seldom reported for layered structure semiconductors, because of their low carrier density (only induced by photo-excitation processes) caused by their low optical absorption which is about 15% for a single layer.[23,30]

Among graphene analogues, titanium disulphide (TiS_2),[31–36] stacked by weak van der Waals (vdW) forces between monolayers, is known to be a suitable thermoelectric material, which has been intensively investigated in the field of condensed matter physics. Unlike graphene, TiS_2 has a giant tunable band gap from ~0.3 eV for bulk structure to ~2.87 eV for a 1–3 layer structure.[34,36] One interesting characteristic of this semiconductor is its in-plane semi-metallic behavior due to its high density of free carriers (10^{20}–10^{21} cm^{-3});[37,38] that is, TiS_2 can easily translate into a plasmon under an external optical field just like metal nanocrystals. In recent years, the transient non-equilibrium states of electrons and holes can be obtained after impulsive excitation of an ultrashort pulse laser in the corresponding electron materials,[29,39] through dramatically increasing the density of carriers. Hence, we infer that, under the intense irradiation of a femtosecond pulse, surface induced non-equilibrium electrons can result in a strong local field which couples with the incident light, subsequently enhancing the nonlinear process as well as producing an ultrafast response, just like that in metal nanocrystals.

To address this challenge, here we used multilayer TiS_2 to study non-equilibrium electron-related optical nonlinearity. Because of the efficient light–matter interaction as well as surface induced non-equilibrium electrons, the transient nonlinear response of a TiS_2 switch is developed, accompanied by a modulation response up to ~145% and a short recovery time of ~768 fs (corresponding to a modulation speed of over 1.3 THz in the intraband transitions of the excited free carriers). As a proof-of-concept demonstration, an all-optical modulation operating near the optical communication band is deployed based on the TiS_2 optical modulator, causing the compression of the continuous laser waves into ultrafast femtosecond laser pulses.

Results and discussion

The samples of TiS_2 used in this work were obtained by liquid phase exfoliation. Unlike other NLO materials, multilayer TiS_2 in solvent can be readily separated into individual layers due to photoinduced separation after pulsed irradiation.[40] Here, TiS_2 flakes distributed on a quartz substrate for NLO measurement, can not only avoid the confusing effect on nonlinear signals, but also imitate the end of a fiber. Fabrication details can be found in the ESI.† As shown by the X-ray diffraction (XRD) results in Fig. 1(a), nearly all of the diffraction peaks, except a broad hump, are congruent with hexagonal TiS_2 according to JPCDS card no. 15-0853.[40] The broad hump range from 10–20° corresponds to quartz glass, while the other main diffraction peaks at 2θ = 34.23, 44.19, 53.83, 56.50, 65.31, and 65.48° can be clearly shown to correspond to (101), (102), (110), (111), (201), and (004), respectively. Characterization by Raman spectroscopy exhibits two main peaks located at ~228.7 cm^{-1} and ~335.8 cm^{-1}, which correspond to E_g (polarization of in-plane vibrations of S normal to the *c*-axis) and A_{1g} (polarization of the vibration of S ions along the *c*-axis) modes,[37,41,42] respectively. Due to strong covalent bonds between the intralayer atoms and weak vdW forces between the layers, the A_{1g} mode is prominent while the E_g mode presents at a much lower intensity, as shown in Fig. 1(b). Atomic force microscopy (AFM) images and height profiles of the prepared TiS_2 samples are representatively shown in Fig. 1(c). The image and the height spectrum indicate that the thickness of TiS_2 is about 55.3 nm, corresponding to ~79 layers of TiS_2. To determine the linear optical response, the absorption spectrum of TiS_2 on a quartz substrate was measured, as shown in Fig. 1(d). The empty quartz substrate serves as a reference. Clearly, a wide frequency range of light (300–2500 nm) can be absorbed by TiS_2. There is a distinguishable peak around ~635 nm, which corresponds to a transition from the 'p' valence band to the lowest-lying 'd_{z^2}' conduction band.[43] X-ray photoelectron spectroscopy (XPS) was also employed to detect the chemical states of surface TiS_2. A detailed view of the XPS pattern in Fig. 1(e) shows that the photoelectron spectrum of Ti 2p contains a spin–orbit of Ti $2p^{3/2}$ and $2p^{1/2}$ centered at ~456.1 eV and ~462.2 eV,[36] while the S 2p spectrum is at ~160.8 eV ($2p^{3/2}$) and ~162.1 eV ($2p^{1/2}$),[44] respectively. Note that there is no other peak or small hump between Ti $2p^{3/2}$ and $2p^{1/2}$, indicating the nonexistence of a TiO_x matrix and the stability of TiS_2.[45] This is in good agreement with previous reported results.

Optical nonlinearity is indispensable for ultrafast laser generation. We characterized the NLO properties of the TiS_2 through a well-developed open-aperture *Z*-scan technique with a femtosecond laser as an excitation source. To identify the measured data more precisely, CS_2 was used as a calibration. More details can be found in the ESI† and in previous work.[10,11,46] Typical NLO behaviors are observed at 800 nm and 1550 nm, as depicted in Fig. 2(a) and (b), respectively, clearly exhibiting SA characteristics; that is, the TiS_2 switch gives an increased transmission as the sample moves from non-focus to on-focus ($z \rightarrow 0$). In addition, the normalized transmissions under different excitation pulse energies have also been exhibited, showing enhanced SA as the focus intensities range from ~28.57 to ~171.4 GW cm^{-2} at 800 nm and from ~0.9885 to ~772.2 GW cm^{-2} at 1550 nm. Notably, there is an absence of any obvious response for the blank quartz slide under the same or even higher excitation intensities, which suggests the significant SA response arises from the

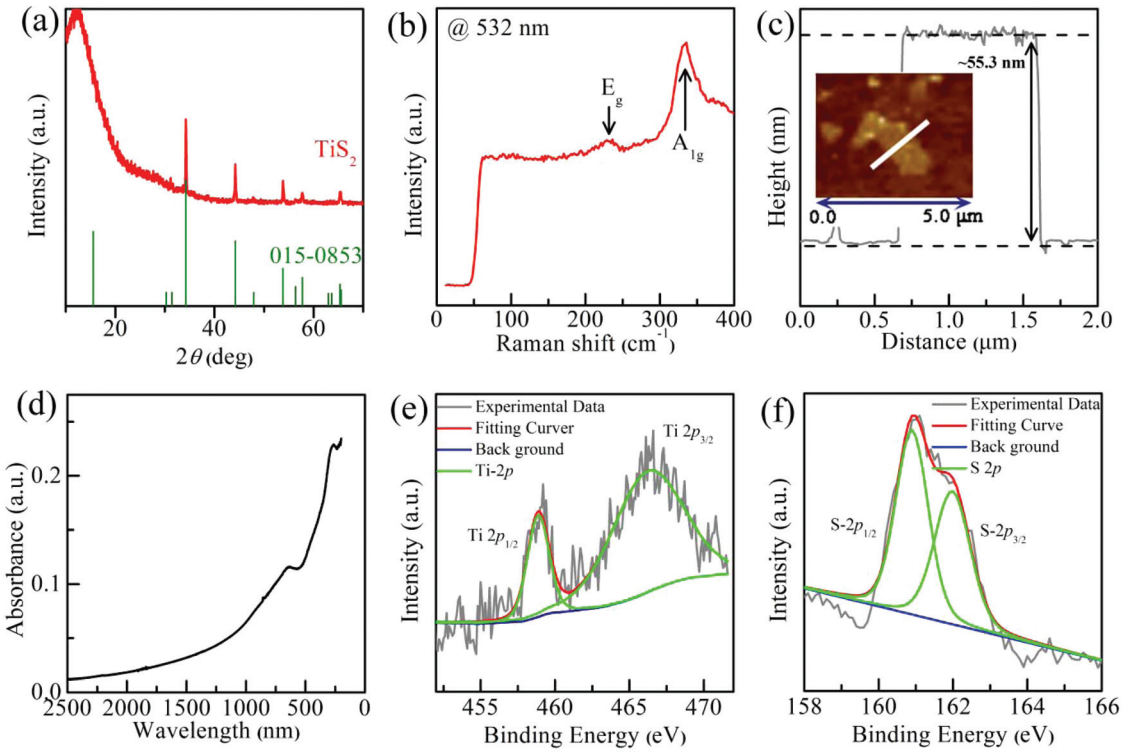

Fig. 1 Characteristics of TiS_2. (a) XRD pattern, clearly showing that all the diffraction peaks are in agreement with JCPDS card no. 15-0853. (b) Raman spectrum excited by a 532 nm laser. (c) AFM height showing the thickness of the as-prepared TiS_2 crystal is about 55.3 nm and the inset is an AFM image. (d) Optical absorption of TiS_2 on the quartz substrate. XPS spectra of TiS_2, where the (e) Ti and (f) S binding energies are identified.

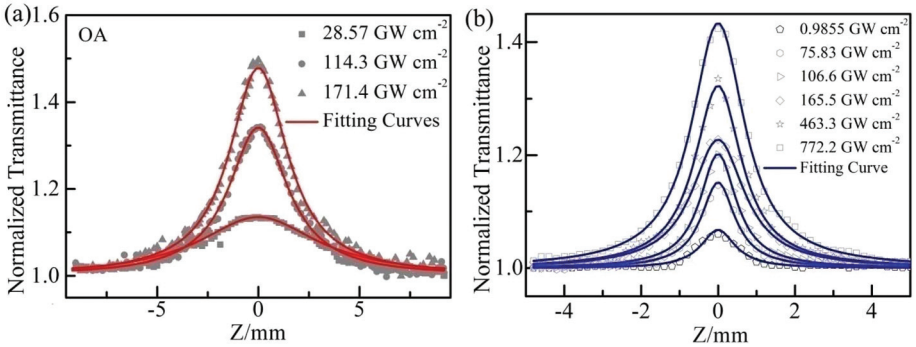

Fig. 2 Open-aperture *Z*-scans of TiS_2 under different excitation wavelengths: (a) 800 nm, and (b) 1550 nm. Normalized transmission *vs.* input power density at different wavelengths: (c) 800 nm, and (d) 1550 nm.

nonlinear modulation effect of TiS_2. This indicates that a low intensity light is effectively suppressed but the absorption decreases while increasing the light intensity. That is to say, the TiS_2 can serve as an ultrafast nonlinear saturable absorber, a passive mode-locking modulator for ultrashort pulsed laser generation in the NIR region. The nonlinear absorption coefficient β is estimated to be $-62.6/-39.0$ cm GW^{-1} at 800/1550 nm (detailed discussion in the ESI†),[10,11] which are orders of magnitude larger than other mono- or few-layer graphene,[47] BPs,[48] and TMDCs such as MoS_2, $MoSe_2$, $MoTe_2$ (see Table S1 for a comparison in the ESI†).[10,17,47] In addition, figures of merit, the NLO refractive index, and third-order NLO susceptibility are also calculated in the ESI.†

In order to unravel the transient dynamic response of the NLO properties in TiS_2, we employed a pump–probe technique to examine the optical response of excited electrons under femtosecond pulse excitation,[49] as shown in Fig. 3(a). Detailed measurement can be found in the ESI.† By increasing the pump power from ~9.89 to ~303.0 μJ cm^{-2}, all of the measurements show a typical optical-induced transparency. The response amplitude increases notably with an increase in the pump power, and can reach up to as large as ~145% at

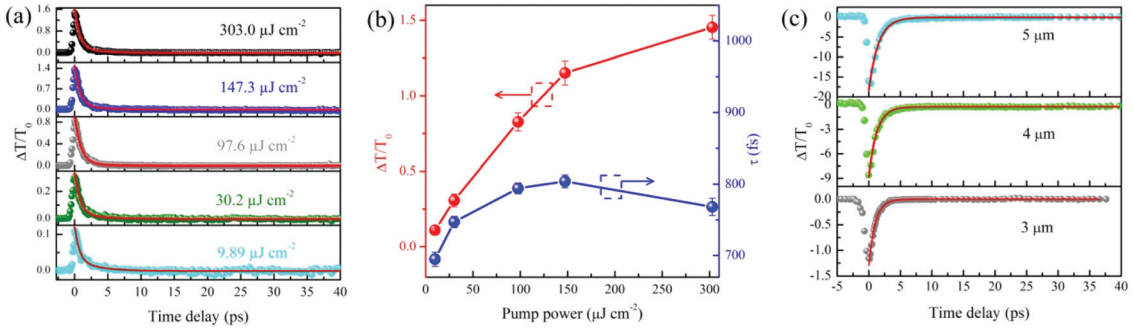

Fig. 3 Ultrafast transient optical response of TiS_2. (a) Transient bleaching dynamics under different pump fluence. (b) Pump fluence-dependent optical response amplitude and recovery time. (c) Transient bleaching dynamics with the probe wavelength of 3.0 μm, 4.0 μm, and 5.0 μm.

~303.0 μJ cm^{-2}, as shown in Fig. 3(b), indicating a superior optical nonlinearity. For multilayer TMDCs, the response decay can be well fitted by a two-temperature model: $y = A_1e^{-x/\tau_1} + A_2e^{-x/\tau_2} + y_0$,[50,51] with a fast component and a slow component, corresponding to carrier–carrier (electron–electron) scattering and carrier–phonon (electron–phonon) scattering, respectively. The recovery time (fast component) as a function of pump fluence is presented in Fig. 3(b). Interestingly, a fluctuation of the recovery time with increasing pump fluence is observed, which may be attributed to a small increase in the electron–phonon coupling time under higher pumping fluence.[52] The fast component is extracted as ~768 ± 12 fs at ~303.0 μJ cm^{-2}, meaning a modulation speed over 1.3 THz, which is slower than graphene (~200 fs)[9] and is comparable to gold nanoparticles (15 nm gold nanoparticles),[25] ITO films/nanorod arrays,[27] and Al-doped ZnO,[28] but faster than monolayer/few-layer MoS_2.[50] In the past decade, lots of investigations on TMDCs such as MoS_2,[50] WS_2,[53] $MoSe_2$,[54] and WSe_2 [51] have revealed that the fast component is on the time scale of picoseconds at room temperature, or even at the lower temperature of liquid nitrogen, indicating a distinct nonlinear progress in the TiS_2 switch because of its sub-picoseconds recovery time. Hence, a detailed discussion about the NLO effect in TiS_2 must be implemented.

Fig. 4(a) shows the usual behavior of photo-excited electrons from the valence band to the conduction band in the semiconductor. Excited by the incident light, electrons from the valence band jump into the conduction band, and almost immediately fill the empty states near the edge of the conduction band, which can block the original interband optical transitions, leading to saturable absorption.[2,10] However, the optical excitation in TiS_2 becomes complex after femtosecond laser irradiation due to its inherent in-plane semi-metallic properties and thermoelectric nature. As shown in Fig. 4(b–d), several processes of electron–electron scattering are possible. Recently, impact ionization has been proven to be a very important process in graphene,[39] and it describes a transition of a second electron across the energy gap caused by an energy transition from a hot electron, leading to an increase in the number of free electrons. The intraband scattering does not

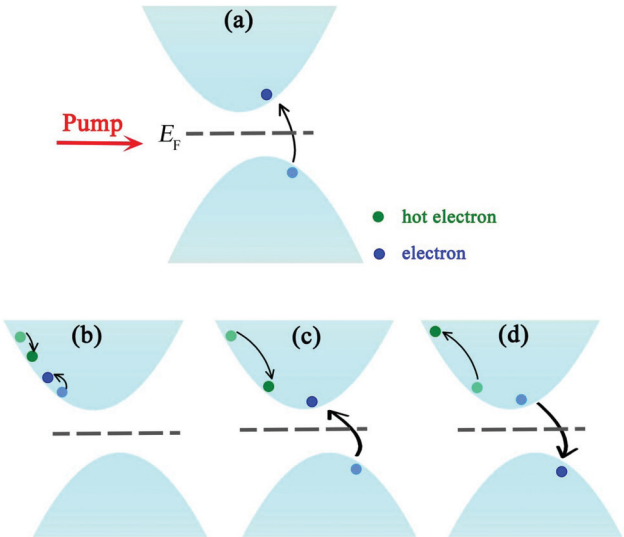

Fig. 4 (a) Photo-excitation induced electron transition from the valence band to the conduction band. The dotted line is the Fermi level. (b–d) Possible electron–electron scattering: intraband scattering (b), interband impact ionization scattering (c) and Auger recombination (d). Impact ionization plays a dominant role in increasing the number of carriers. The intraband scattering, Auger recombination, and electron–phonon scattering cannot cause an increase of carriers. The solid green circle presents hot electrons with high energy, while the blue one presents electrons.

directly increase the density of electrons; however, it can stimulate the electrons with low energy to jump to higher energy states, leading to the increase of hot electrons. In addition, more electrons in the valence band can be pumped into the conduction band due to a decrease of electrons with low energy in the conduction.[39] Since there are abundant free photons in the conduction band after strong irradiation using a femtosecond pulse, electrons in the conduction band can also transfer to higher states through free carrier absorption (FCA).[29] It is difficult to increase the density of electrons (to induce plasma regime) through only the photon-excitation transition described in Fig. 4(a), because of the low electron saturable threshold which can be easily reached under the

excitation of a femtosecond pulse to present typical SA response.[10,14–16,29] To date, the highest electron density (10^{-13} cm^{-2}) in TMDCs is only observed for monolayer WS_2 under femtosecond pulse irradiation, leading to a Mott transition from an insulating semiconductor regime to an electron–hole plasma regime. Interestingly, the electron–electron scattering time (the recovery time) is estimated to be ~400 fs in the plasma regime of monolayer WS_2 after a Mott transition,[29] which is faster than the dynamic process (several picoseconds) without undergoing a Mott transition (non-plasma regime); that is, the plasma regime enhances the light–matter interactions compared to the semiconductor regime.[3] For semi-metallic materials, the density of electrons can easily increase through the synergistic processes of impact ionization and intraband scattering to enhance light–matter coupling. S. Mathias *et al.* reported a strong increase in the number of carriers from impact ionization on the timescale of ~200 fs in an 80 nm thin single-crystal of $TiSe_2$ under a NIR pump using femtosecond time-domain spectroscopy.[39] Based on the $TiSe_2$ experiment (similar electron materials with TiS_2), we can reasonably assume a non-equilibrium distribution of electrons from electron–electron scattering events in the initial stage after a femtosecond pumping. This non-equilibrium distribution will take hundreds of femtoseconds (~768 fs) to be thermalized into a hot electron, in which intraband scattering and impact ionization play a dominant role, like $TiSe_2$ and graphene.[39] The dramatic increase in the number of carriers transforms the dull TiS_2 into a plasma with a high density of surface electrons (electron wave functions) after impulsive femtosecond excitation. These dense electrons induce a surface longitudinal field (a local electromagnetic field) to arise from vertical bonds between neighboring planes.[35] The plasmonic excitations can finally boost high-order nonlinear progress in TiS_2 (see section 1 in the ESI†), leading to an ultrafast response (~768 fs) and a large modulation amplitude (~145%), as shown in Fig. 3, differing from other semiconductors (MoS_2, $MoSe_2$, *etc.*).[50,54] Here, the non-equilibrium distribution of electrons can disturb the band edge (Femi energy)[29] and further perturb the photo-excitation process (Fig. 4a). Nonetheless, the surface plasmonic states are still formed under strong photoexcitation, because of the dominance of impact ionization and its inherent in-plane semi-metallic properties, as well as the thermoelectric nature of TiS_2. For plasmonic nanocrystals, such as Au nanoparticles, Wang *et al.* reported a transition from saturable to reverse-saturable absorption when the irradiation intensity increased to ~5 GW cm^{-2},[26] which is in accordance with other work. But for a TiS_2 absorber, benefitting from the bistability of a semiconductor and a semi-metal, SA behavior is still shown even at a high irradiation intensity (~772.2 GW cm^{-2}), differing from plasmonic nanocrystals. Also, according to the report on black phosphorus dispersions in NMP by Huang *et al.*,[55] a transition from a SA response at low excitation fluence to an optical limiting response at high excitation was recorded, which is induced by microbubbles by thermal effects to scatter most of the ultrafast laser. In this work, TiS_2 is dispersed on a quartz slide to imitate optical fiber facing, effectively avoiding the influence on the NLO response from other negative factors and so that TiS_2 can still exhibit a SA response under high power density. Therefore, the ultrafast nonlinear process depends not only on the band structure, but also on the non-equilibrium distribution of electrons. In order to verify this point of view, the pump–probe under a long wavelength (from 3.0 μm to 5.0 μm to make sure the SA signal was reversed) was then measured,[56] as shown in Fig. 3(c). The typical reverse saturable absorption behaviors as well as the ultrafast dynamics also indicate the synergy between the band structure and the non-equilibrium electrons. More discussion can be found in the ESI.† The diversities of the semiconductor and semi-metal in TiS_2 lay the foundation for the potential application of ultrashort pulse generation.

The ultrafast transient bleach dynamic response and strong nonlinear optical modulation in TiS_2 prompt us to further explore their capability towards all-optical modulating applications for nonlinear pulse reshaping. Here, in the proof-of-concept demonstration, the fiber modulator is integrated with a fiber structure to operate as a femtosecond mode-locked Er-doped fiber laser near the optical communication band, as shown in Fig. 5(a), switching continuous laser waves into laser pulses (more details can be found in the ESI†). As a reference, the laser cavity was tested without constructing TiS_2 samples, and only continuous waves can be observed. In our experiment, the laser oscillation started initially for a continuous wave lasing at a low pump threshold of ~16 mW. The pump power was increased to ~21.5 mW to optimize the mode locking operation. Once a stable output was recorded, no further polarization controller (PC) for adjusting the polarization state of light was used. Fig. 5(b) shows a typical mode-locking output spectrum centered at ~1544.5 nm, with a soliton-like pulse generated from intracavity periodical perturbations.[9] Shown in Fig. 5(c), the laser delivered the oscilloscope trace of the output pulse-train with a period of ~175.5 ns, corresponding to a repetition rate of ~5.70 MHz, as expected from the cavity round-trip time. Importantly, a stable femtosecond pulse with signal-to-noise of ~70 dB (see Fig. S6 in the ESI†) and temporal width of ~618 fs (assuming a $Sech^2$ pulse shape, pulse duration is 402 fs) can be extracted from the auto-correlation trace in Fig. 5(d). The performance of the TiS_2 mode-locked laser near the telecommunication range of ~1550 nm, is comparable to that which has previously been achieved with MoS_2,[10] graphene[8], and SWNTs,[6] which is triggered by the interaction of dispersion management of the waveguide and nonlinearity of TiS_2 as well as the enhanced light–matter interaction. However, a wideband operation can be achieved with as-prepared TiS_2, with an enhanced photon-induced interaction compared to graphene or few-layer MoS_2;[8,30] with no need for special procedures of diameter or chirality as with SWNTs.[6] Furthermore, the femtosecond temporal width could bring new opportunities for medical imaging, micromachining, precision measuring, as well as telecommunications, *etc.*

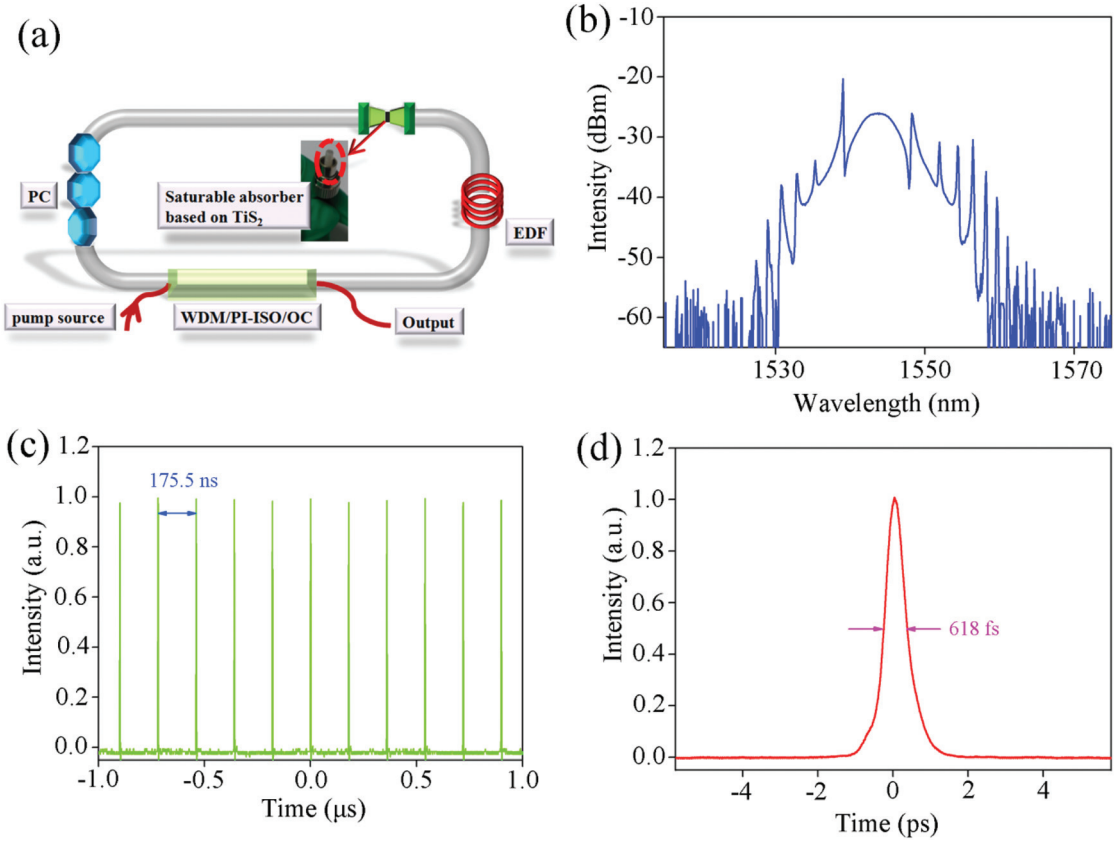

Fig. 5 Ultrafast all-optical switching enabled by a TiS_2 switch near the optical communication band. (a) Schematic illustration of the experiment setup. (b) Mode-locked optical spectrum. (c) Mode-locked pulse trains. (d) Temporal width of one pulse.

Conclusion

In summary, multilayer TiS_2 is prepared through facile liquid phase exfoliation and can be used as an effective optical modulator for ultrafast optical laser generation near the optical communication band due to non-equilibrium electron induced ultrafast nonlinear optical response. Broadband nonlinear saturable absorption is recorded in the NIR region with a larger modulation response up to ~145% and an ultrafast recovery time of ~768 fs (corresponding to the modulation speed of over 1.3 THz). Furthermore, a stable femtosecond mode-locking spectrum with soliton pulses is observed with a duration of ~402 fs using a TiS_2-based modulator, and a pulse train duration of ~175.5 ns. This successful modulation provides a valuable strategy and opens new avenues toward advanced photonic devices based on TiS_2 nonlinear material.

Methods

Sample preparation, characterization, *Z*-scan measurements, pump–probe measurement and ultrafast pulse generation can be found in the ESI.†

Conflicts of interest

There are no conflicts to declare.

Acknowledgements

This work was financially supported by the National Key R&D program of China (Grant No. 2018YFB1107200), the National Natural Science Foundation of China (Grant No. 51472091, 51772270, 51302087) and the Guangdong Natural Science Foundation (Grant No. S2011030001349). This work was also supported by the Natural Science Foundation of Zhejiang Province (Grant No. LQ18A040004) and the Open Fund of the State Key Laboratory of Luminescent Materials and Devices (South China University of Technology, Grant No. 2018-skllmd-13).

References

1 R. W. Boyd, in *Nonlinear Optics*, Academic Press, Burlington, USA, 3rd edn, 2008.
2 U. Keller, *Nature*, 2003, **424**, 831–838.
3 M. Kauranen and A. V. Zayats, *Nat. Photonics*, 2012, **6**, 737–748.

4 P. A. Franken, A. E. Hill, C. W. Peters and G. Weinreich, *Phys. Rev. Lett.*, 1961, **7**, 118–119.
5 S. Colin, E. Contesse, P. Le Boudec, G. Stephan and F. Sanchez, *Opt. Lett.*, 1996, **21**, 1987–1989.
6 T. Hasan, Z. Sun, F. Wang, F. Bonaccorso, P. H. Tan, A. G. Rozhin and A. C. Ferrari, *Adv. Mater.*, 2009, **21**, 3874–3899.
7 A. Haboucha, V. Fortin, M. Bernier, J. Genest, Y. Messaddeq and R. Vallée, *Opt. Lett.*, 2014, **39**, 3294–3297.
8 Q. Bao, H. Zhang, Y. Wang, Z. Ni, Y. Yan, Z. X. Shen, K. P. Loh and D. Y. Tang, *Adv. Funct. Mater.*, 2009, **19**, 3077–3083.
9 Z. Sun, T. Hasan, F. Torrisi, D. Popa, G. Privitera, F. Wang, F. Bonaccorso, D. M. Basko and A. C. Ferrari, *ACS Nano*, 2010, **4**, 803–810.
10 R. Wei, H. Zhang, X. Tian, T. Qiao, Z. Hu, Z. Chen, X. He, Y. Yu and J. Qiu, *Nanoscale*, 2016, **8**, 7704–7710.
11 R. Wei, H. Zhang, Z. Hu, T. Qiao, X. He, Q. Guo, X. Tian, Z. Chen and J. Qiu, *Nanotechnology*, 2016, **27**, 305203.
12 H. Zhang, X. He, W. Lin, R. Wei, F. Zhang, X. Du, G. Dong and J. Qiu, *Opt. Express*, 2015, **23**, 13376–13383.
13 H. Mu, S. Lin, Z. Wang, S. Xiao, P. Li, Y. Chen, H. Zhang, H. Bao, S. P. Lau, C. Pan, D. Fan and Q. Bao, *Adv. Opt. Mater.*, 2015, **3**, 1447–1453.
14 J. Koo, Y. I. Jhon, J. Park, J. Lee, Y. M. Jhon and J. H. Lee, *Adv. Funct. Mater.*, 2016, **26**, 7454–7461.
15 D. Mao, B. Du, D. Yang, S. Zhang, Y. Wang, W. Zhang, X. She, H. Cheng, H. Zeng and J. Zhao, *Small*, 2016, **12**, 1489–1497.
16 Z. Luo, Y. Li, M. Zhong, Y. Huang, X. Wan, J. Peng and J. Weng, *Photonics Res.*, 2015, **3**, A79–A86.
17 K.-G. Zhou, M. Zhao, M.-J. Chang, Q. Wang, X.-Z. Wu, Y. Song and H.-L. Zhang, *Small*, 2015, **11**, 694–701.
18 M. He, C. Quan, C. He, Y. Huang, L. Zhu, Z. Yao, S. Zhang, J. Bai and X. Xu, *J. Phys. Chem. C*, 2017, **121** 27147–27153.
19 M. Zhang, G. Hu, G. Hu, R. C. T. Howe, L. Chen, Z. Zheng and T. Hasan, *Sci. Rep.*, 2015, **5**, 17482.
20 K. Wang, J. Wang, J. Fan, M. Lotya, A. O'Neill, D. Fox, Y. Feng, X. Zhang, B. Jiang, Q. Zhao, H. Zhang, J. N. Coleman, L. Zhang and W. J. Blau, *ACS Nano*, 2013, **7**, 9260–9267.
21 J. Zhang, D. Li, R. Chen and Q. Xiong, *Nature*, 2013, **493**, 504.
22 D. Li, J. Zhang and Q. Xiong, *Opt. Express*, 2013, **21**, 19302–19310.
23 S. Wang, H. Yu, H. Zhang, A. Wang, M. Zhao, Y. Chen, L. Mei and J. Wang, *Adv. Mater.*, 2014, **26**, 3538–3544.
24 Z. Liu, H. Mu, S. Xiao, R. Wang, Z. Wang, W. Wang, Y. Wang, X. Zhu, K. Lu, H. Zhang, S.-T. Lee, Q. Bao and W. Ma, *Adv. Mater.*, 2016, **28**, 3535–3542.
25 S. Link, C. Burda, Z. L. Wang and M. A. El-Sayed, *J. Chem. Phys.*, 1999, **111**, 1255–1264.
26 S. Wang, Y. Zhang, R. Zhang, H. Yu, H. Zhang and Q. Xiong, *Adv. Opt. Mater.*, 2015, **3**, 1342–1348.
27 M. Z. Alam, I. De Leon and R. W. Boyd, *Science*, 2016, **352**, 795–797.
28 P. Guo, R. D. Schaller, J. B. Ketterson and R. P. H. Chang, *Nat. Photonics*, 2016, **10**, 267–273.
29 A. Chernikov, C. Ruppert, H. M. Hill, A. F. Rigosi and T. F. Heinz, *Nat. Photonics*, 2015, **9**, 466.
30 Y. Li, A. Chernikov, X. Zhang, A. Rigosi, H. M. Hill, A. M. van der Zande, D. A. Chenet, E.-M. Shih, J. Hone and T. F. Heinz, *Phys. Rev. B: Condens. Matter Mater. Phys.*, 2014, **90**, 205422.
31 C. Tan, Z. Lai and H. Zhang, *Adv. Mater.*, 2017, **29**, 1701392.
32 C. Wan, X. Gu, F. Dang, T. Itoh, Y. Wang, H. Sasaki, M. Kondo, K. Koga, K. Yabuki, G. J. Snyder, R. Yang and K. Koumoto, *Nat. Mater.*, 2015, **14**, 622.
33 X. Li, X. Ding, Y. Li, L. Wang and J. Fan, *Nanoscale*, 2016, **8**, 9852–9860.
34 S. J. Varma, J. Kumar, Y. Liu, K. Layne, J. Wu, C. Liang, Y. Nakanishi, A. Aliyan, W. Yang, P. M. Ajayan and J. Thomas, *Adv. Opt. Mater.*, 2017, **5**, 1700713.
35 D. Samuelsen, E. Pehlke, W. Schattke, O. Anderson, R. Manzke and M. Skibowski, *Phys. Rev. Lett.*, 1992, **68**, 522–525.
36 T. Li, Y.-H. Liu, B. Chitara and J. E. Goldberger, *J. Am. Chem. Soc.*, 2014, **136**, 2986–2989.
37 S. J. Sandoval, X. K. Chen and J. C. Irwin, *Phys. Rev. B: Condens. Matter Mater. Phys.*, 1992, **45**, 14347–14353.
38 P. C. Klipstein, A. G. Bagnall, W. Y. Liang, E. A. Marseglia and R. H. Friend, *J. Phys. C: Solid State Phys.*, 1981, **14**, 4067.
39 S. Mathias, S. Eich, J. Urbancic, S. Michael, A. V. Carr, S. Emmerich, A. Stange, T. Popmintchev, T. Rohwer, M. Wiesenmayer, A. Ruffing, S. Jakobs, S. Hellmann, P. Matyba, C. Chen, L. Kipp, M. Bauer, H. C. Kapteyn, H. C. Schneider, K. Rossnagel, M. M. Murnane and M. Aeschlimann, *Nat. Commun.*, 2016, **7**, 12902.
40 D. Rossi, J. H. Han, D. Yoo, Y. Dong, Y. Park, J. Cheon and D. H. Son, *J. Phys. Chem. C*, 2014, **118**, 12568–12573.
41 S. Dhavala, V. Siva, J. Shalikram, S. Kartik, S. Pratap Kumar, V. Shikha and P. Ram Shanker, *J. Phys.: Condens. Matter*, 2017, **29**, 485708.
42 X. Zhang, Q.-H. Tan, J.-B. Wu, W. Shi and P.-H. Tan, *Nanoscale*, 2016, **8**, 6435–6450.
43 A. M. Ghorayeb and R. H. Friend, *J. Phys. C: Solid State Phys.*, 1987, **20**, 4181.
44 J. Kibsgaard, Z. Chen, B. N. Reinecke and T. F. Jaramillo, *Nat. Mater.*, 2012, **11**, 963.
45 H. Martinez, C. Auriel, D. Gonbeau, M. Loudet and G. Pfister-Guillouzo, *Appl. Surf. Sci.*, 1996, **93**, 231–235.
46 R. Wei, X. Tian, Z. Hu, H. Zhang, T. Qiao, X. He, Q. Chen, Z. Chen and J. Qiu, *Opt. Express*, 2016, **24**, 25337–25344.
47 K. Wang, Y. Feng, C. Chang, J. Zhan, C. Wang, Q. Zhao, J. N. Coleman, L. Zhang, W. J. Blau and J. Wang, *Nanoscale*, 2014, **6**, 10530–10535.
48 Y. Wang, G. Huang, H. Mu, S. Lin, J. Chen, S. Xiao, Q. Bao and J. He, *Appl. Phys. Lett.*, 2015, **107**, 091905.

49 C. Zhu, F. Wang, Y. Meng, X. Yuan, F. Xiu, H. Luo, Y. Wang, J. Li, X. Lv, L. He, Y. Xu, J. Liu, C. Zhang, Y. Shi, R. Zhang and S. Zhu, *Nat. Commun.*, 2017, **8**, 14111.
50 Q. Wang, S. Ge, X. Li, J. Qiu, Y. Ji, J. Feng and D. Sun, *ACS Nano*, 2013, **7**, 11087–11093.
51 C. Poellmann, P. Steinleitner, U. Leierseder, P. Nagler, G. Plechinger, M. Porer, R. Bratschitsch, C. Schüller, T. Korn and R. Huber, *Nat. Mater.*, 2015, **14**, 889.
52 B. T. Diroll, P. Guo, R. P. H. Chang and R. D. Schaller, *ACS Nano*, 2016, **10**, 10099–10105.
53 L. Yang, N. A. Sinitsyn, W. Chen, J. Yuan, J. Zhang, J. Lou and S. A. Crooker, *Nat. Phys.*, 2015, **11**, 830.
54 A. Singh, G. Moody, S. Wu, Y. Wu, N. J. Ghimire, J. Yan, D. G. Mandrus, X. Xu and X. Li, *Phys. Rev. Lett.*, 2014, **112**, 216804.
55 J. Huang, N. Dong, S. Zhang, Z. Sun, W. Zhang and J. Wang, *ACS Photonics*, 2017, **4**, 3063–3070.
56 Y. Ge, Z. Zhu, Y. Xu, Y. Chen, S. Chen, Z. Liang, Y. Song, Y. Zou, H. Zeng, S. Xu, H. Zhang and D. Fan, *Adv. Opt. Mater.*, 2018, **6**, 1701166.

